RSC Advances

PAPER

View Article Online
View Journal | View Issue

Cite this: *RSC Adv.*, 2020, **10**, 23016

Sensitivity enhancement *via* multiple contacts in the {^{1}H–^{29}Si}–^{1}H cross polarization experiment: a case study of modified silica nanoparticle surfaces†

Chuanyu Yan,[ab] François Kayser[c] and Reiner Dieden *[a]

Received 7th February 2020
Accepted 10th June 2020

DOI: 10.1039/d0ra04995f

rsc.li/rsc-advances

{^{1}H–^{29}Si}–^{1}H double cross polarization inverse detection (DCPi) solid-state NMR, has recently been shown to be a powerful tool for studying molecules adsorbed on the silica surface. In this contribution, we develop an improved version (MCPi) which incorporates a block of multiple contact pulses, and quantitatively compare the sensitivities of MCPi and DCPi over a typical range of experimental parameters. The MCPi pulse sequence aims at higher sensitivity and robustness for studying samples with various relaxation characteristics. In the case of dimethyl sulfoxide (DMSO) molecules adsorbed on the silica surface, MCPi performs equally well or up to 2.5 times better than DCPi over a wide range of parameters. The applicability to and performance of MCPi on composite materials was demonstrated using a sample of polymer–silica composite, where significantly higher sensitivity could be achieved at very long total mixing times. The results also showed that both techniques are surface specific in the sense that only the groups close to the surface can be detected.

1. Introduction

Understanding the chemistry occurring on surfaces and at interfaces plays a critical role in materials science. For example, it helps to rationalize the mechanism of catalytic reactions,[1–4] to improve the performance of anode/cathode materials in energy devices,[5–7] to increase the separation efficiency of chromatography[8,9] and to compatibilize different phases in composite materials.[10–12] Silica, *e.g.*, in addition to serving as a support material in materials science,[4,13,14] has also been used for drug-delivery systems through either inclusion[16] or adsorption[17] of the active ingredient. However, while many of the spectroscopic techniques available today are very powerful for analysing bulk properties, it is still non-trivial to obtain surface-specific chemical information.

1.1 Study of silica by ^{29}Si solid-state NMR

Silica and its surface have been studied extensively using a wide array of solid-state NMR (ssNMR) techniques that have revealed the presence of water and several hydroxy (silanol) species, involved to different degrees in hydrogen bonding.[15,18–20]

For the characterization of silica and silicate surfaces, ^{29}Si cross polarisation under magic angle spinning solid-state nuclear magnetic resonance spectroscopy (^{29}Si CP/MAS ssNMR) has proven to be a valuable tool.[15,20–24] Although direct polarisation (DP) can also provide valuable information its use is hampered by very long spin–lattice (T_1) relaxation times.[25,26]

If the Hartmann–Hahn matching condition $\omega_I = \omega_S$ is met, the polarisations of two nuclear species can equilibrate through dipolar coupling. If the polarisations are different, this cross-polarisation (CP) can lead to an enhancement of the lowest population by a factor of γ_I/γ_S (γ is the gyromagnetic ratio of the isotope).

The efficiency of CP depends essentially on two parameters, the rotating frame relaxation ($T^I_{1\rho}$) of the reservoir species (*e.g.* ^{1}H), and the cross-polarisation constant, T_{IS}. Since T_{IS} can be very different for different I–S pair in the same sample, a single setting of CP parameters is not optimal for all S nuclei of the sample in most cases.

As improvements on the simple CP experiment, schemes involving multiple CP contacts have been proposed, mostly aiming at generating a more even signal enhancement and quantitative response.[27–29]

While the theoretical maximum enhancement (*i.e.* $\gamma_{1H}/\gamma_{29Si}$) is rarely achieved by one single CP step, it has been shown that multiple-step CP (multiCP) can significantly enhance the

[a]*Luxembourg Institute of Science and Technology, Department of "Materials Research and Technology", Avenue des Hauts-Fourneaux, L-4362 Esch-sur-Alzette, Luxembourg. E-mail: reiner.dieden@list.lu; Fax: (+352) 275 885; Tel: (+352) 275 888 4576*

[b]*University of Luxembourg, Faculty of Science, Technology and Communication, Avenue des Hauts-Fourneaux, L-4365 Esch-sur-Alzette, Luxembourg*

[c]*Goodyear Innovation Center Luxembourg, Avenue Gordon Smith, L-7750 Colmar-Berg, Luxembourg*

† Electronic supplementary information (ESI) available. See DOI: 10.1039/d0ra04995f

magnetisation for species with unequal cross-relaxation characteristics.[28]

In multiCP, the X nucleus magnetization can be pushed closer and closer to the maximum enhancement with increasing number of contacts, eventually achieving a homogeneous enhancement for all X-nuclei *via* multiple CP steps. The multiCP experiment was initially designed to obtain quantitative X nucleus response.[28–30] Nevertheless, there are recent reports of using a multiCP block for the purpose of sensitivity enhancement.[31,32]

1.2 Surface specific techniques

Approaches to achieve surface specific detection in solid state NMR encompass the use of relaxation agents,[26] ^{29}Si DNP,[33,34] and ^{17}O DNP.[35,36] Nevertheless, regular CP can be considered to be a surface selective technique, provided that the protons are occurring exclusively at the surface of the silica particle.[20,37]

This is because magnetization transfer *via* CP relies on through-space dipolar couplings, the strength of which is proportional to $1/r^3$ (r is the distance between the dipolar coupled spin pair). Hence, the information derived from CP ssNMR is usually limited to a region of a few nanometers.[38] The dipolar coupled protons and silicon atoms have been investigated by 2D ^{1}H–^{29}Si heteronuclear correlation (HETCOR) on the silicon[39] and silica[19,38,40–42] surfaces.

Similarly, X-filtered double-cross polarisation experiments have been reported to specifically record spectra of X-nuclei of small molecules in the indirect dimension of a 2D experiment. This technique consists of two distinct CP periods during the first of which magnetisation is transferred from ^{1}H to the X nucleus, from where it is then back-transferred to proton *via* the second CP block.[43–48]

A 1D version of this experiment, $\{^1$H–^{29}Si$\}$–^{1}H double cross polarization inverse detection (DCPi), has recently been applied to the study of molecules adsorbed on the silica and silicate surfaces.[38,49–52] The $\{^1$H–^{29}Si$\}$–^{1}H DCPi experiment[38] consists of three steps. First, a ^{1}H → ^{29}Si CP period (t_{cp1}) ensures the surface ^{29}Si magnetization is established. Second, a train of 90° excitation pulses is used to saturate the ^{1}H magnetization so that no transverse magnetization, due to direct excitation during the second spin lock period (t_{cp2}), could be detected in the final spectrum. During the proton saturation period, the ^{29}Si magnetization is stored on the longitudinal axis. In the third step, the ^{29}Si magnetisation is rotated back onto the transverse plane by a 90° pulse and then, during the second cross-polarization period (t_{cp2}), transferred back only to those ^{1}H spins that are within reach, *i.e.* close to the surface. Because of its dependence on the ^{1}H–^{29}Si dipolar couplings, the intensity of the ^{1}H signal depends on the inter-nuclear distance, although proton–proton spin diffusion can also interfere, which can be minimized by using short contact times (t_{cp2}). By applying this approach one can tell whether a molecule/functional group is on (or close to) the silica surface.

This $\{^1$H–^{29}Si$\}$–^{1}H DCPi technique could provide information complementary to other sensitivity-enhanced techniques (X-nucleus detected) such as the Carr–Purcell–Meiboom–Gill (CPMG)[34,40,41,53,54] and dynamic nuclear polarization techniques (DNP).[33,34,55–57] In terms of silica/silicate materials, the former can reveal the local proton environments on the surface, while the latter can provide information about the silicon groups of silica and silicates.

In addition to the applications reported so far, the $\{^1$H–^{29}Si$\}$–^{1}H DCPi technique also has the potential to study competitive adsorption phenomena on the surface of silica and silicate, which is an important and challenging topic.[58] These ubiquitous phenomena can occur, for example, among small molecules,[59–62] among polymers[63,64] and between polymer and surfactant.[65,66]

In order to further improve the sensitivity of this surface-specific technique for composite materials with a rather low silica content or nanoparticles with a relatively low surface loading,[17,56,67,68] where even slight sensitivity improvement could reduce experiment time significantly, we report here a modified version of DCPi. This new version, multiple contact cross polarization inverse detection ssNMR (MCPi), uses a multiCP block to enhance the polarisation build-up during the initial CP period. Its sensitivity is quantitatively compared to that of DCPi over a typical range of conditions.

One of the reasons for replacing the first CP step of DCPi with a block of multiple CP steps is because it is expected to further push the ^{29}Si magnetization towards the maximum level ($\gamma_{1H}/\gamma_{29Si}$).

Another reason for inserting the multiCP block is its robustness, *i.e.* its capability of achieving strong enhancements for spins with different cross-polarisation kinetics.[28] Although it has always been assumed that $T_{1\rho}^{I} > T_{IS}$, the situation can be the opposite in some cases, *i.e.* $T_{1\rho}^{I} < T_{IS}$.[69] To cover a wide range of relaxation characteristics, *e.g.* as for the different types of hydroxyl groups at the silica surface, without the need of putting too much effort on measuring the $T_{1\rho}^{I}$ and T_{IS} for every sample, multiCP can safely enhance the magnetization without losing it due to $T_{1\rho}^{I}$.

2. Experimental

2.1 Materials

The materials used in this work were obtained from the following sources with given specifications. Silica nanoparticle (SiNP) (Sigma-Aldrich, product no. 637246, 99.5% particle size 5–15 nm (TEM), surface area 590–690 m^2 g^{-1} (TEM)); Pure water (resistance 18.2 MΩ, purified by Simplicity® water purification system, Millipore S.A.S, France); dimethyl sulfoxide (DMSO-h$_6$, from ACROS Organics, >99.7%); deuterated dimethyl sulfoxide (DMSO-d$_6$, from ACROS Organics, 99.8% deuterium); deuterated chloroform ($CDCl_3$, Aldrich, >99.8%D).

2.2 Preparation of DMSO-adsorbed SiNP

Individual chemicals were used as received. In addition, the DMSO-adsorbed SiNP was prepared in the following way. (1) 0.20 gram of silica was mixed with 0.11 gram of DMSO-h$_6$ or DMSO-d$_6$ in the suspension of 5 mL of $CDCl_3$ under magnetic stirring overnight at a speed of 300 rpm at room temperature.

(2) The mixture was then subjected to high speed centrifuging at 12 000 rpm for 10 minutes. (3) Afterwards, the DMSO-adsorbed SiNPs were dried in a warm air-circulating oven at 50 °C for 1 hour.

2.3 Preparation of polymer–silica composite

1 gram of silica (Zeosil® Premium 200MP, Solvay) was reacted overnight with 20 mL of trimethylchlorosilane (≥98.0%, Sigma Aldrich) in a round bottom flask on a magnetic stirrer at room temperature. Then, the flask was opened to air to let the unreacted silane, formed hydrochloric acid and silane dimer evaporate at room temperature in a fume hood for about one day. The silanized silica was then mixed with polyisoprene (LIR-10, Kuraray) – (mass ratio ~ 100 : 80) in deuterated chloroform and the chloroform removed by oven-drying at 50 °C.

2.4 ssNMR experiments

The details about the pulse sequences of $\{^1H–^{29}Si\}–^1H$ DCPi/MCPi, $\{^1H\}–^{29}Si$ multiCP and $^1H–^1H$ RFDR are provided in Fig. S1.† In addition, routine experiments such as ^{29}Si direct polarization (DP) under high power decoupling and ^1H one-pulse were also performed.

The solid samples were loaded into a 4 mm zirconium oxide (ZrO_2) rotor with a Kel-F cap, while the liquid samples were loaded in a Kel-F HR-MAS insert, which was then inserted into the ZrO_2 rotor. The rotors were spun at a MAS speed of 14 kHz (unless noted otherwise) at 303 K in a double resonance probe of a Bruker Avance III HD 600 MHz spectrometer, controlled by TopSpin 3.5pl7 software. The chemical shifts reported here were externally referenced *vs.* pure TMS by setting the methylene carbon of adamantane to 38.48 ppm. The ^1H and ^{29}Si 90° pulse lengths were 2.9 and 5.0 microseconds, respectively. In cross polarization experiments, the spin locking strength of ^{29}Si was set to 50 kHz while that of ^1H was a shaped ramp from 34 to 66 kHz. The number of scans (NS) for the $\{^1H–^{29}Si\}–^1H$ DCPi/MCPi and $\{^1H\}–^{29}Si$ multiCP were 2048, the recycle delay (RD) was 4.0 seconds and acquisition time was 50 ms, unless noted otherwise. For the saturation train in DCPi and MCPi, we used 64 saturation pulses separated by a delay (τ_{sat}) of 1 ms, unless noted otherwise. In the MCPi experiments of the polymer–silica compound, the saturation scheme of Fig. 1B was replaced with two long low-power pulses (pulse length = 500 ms at a power level of 1 watts) with a 90°-phase shift, because even a train of 512 saturation pulses (inter-pulse delay τ_{sat} = 1 ms) was found to be insufficient for obtaining a clean background. For $^1H–^1H$ RFDR, the following acquisition parameters were used: RD = 4.0 seconds, mixing time = 18 ms, 128 increments on the indirect dimension and NS = 16. For the ^{29}Si DP experiment at natural abundance, note that the T_1 of ^{29}Si is so long that our attempt to measure it in a practical timeframe was not successful. Thus, a RD of 120 s that is quite common in literature,[16] was used here.

The signal-to-noise ratio (S/N) was calculated in TopSpin using the Bruker command "SINO" with the signal and noise ranges defined in Tables S1 and S2.† To make fair comparisons, the $\{^1H$ –$^{29}Si\}–^1H$ DCPi and MCPi spectra were processed using the same processing parameters (512 time domain points, without apodization and fixed regions for calculating S/N ratio).

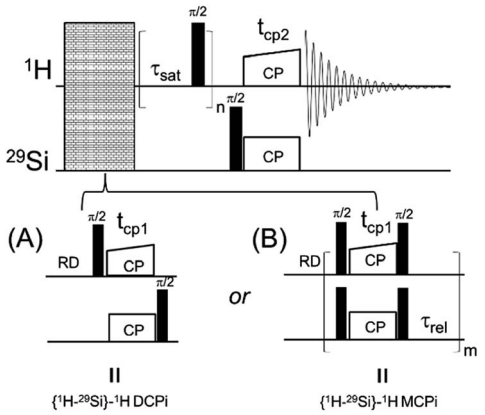

Fig. 1 The diagrams of two solid-state NMR pulse sequences. (A) $\{^1H–^{29}Si\}–^1H$ double cross polarization inverse detection (DCPi). (B) $\{^1H–^{29}Si\}–^1H$ multiple cross polarization inverse detection (MCPi).

3. Results and discussion

3.1 A case study of DMSO adsorption

In order to compare the sensitivities of the two sequences, $\{^1H–^{29}Si\}–^1H$ DCPi (Fig. 1A) and $\{^1H–^{29}Si\}–^1H$ MCPi (Fig. 1B), we used a surface modified silica nanoparticle. In this model sample, dimethyl sulfoxide (DMSO, a strong hydrogen bonding acceptor known to displace other molecules on the silica[63]) was used to displace the ubiquitous physically adsorbed water on the surface of silica nanoparticles (SiNP) (Fig. 2A). DMSO has a single methyl proton resonance far away from the silanol and water peaks, which allows to make unambiguous assignments. In order to be able to assign the ^1H chemical shifts to each surface molecule/group (Fig. 2B), the ^1H one-pulse experiments were compared with those of the individual materials as well as the mixtures (Fig. S3†). The ^1H peak at 3.16 ppm was assigned to the protons of DMSO because this peak vanished when using deuterated DMSO. The broad ^1H peaks at 7.5 ppm and at 5.0 ppm were assigned to hydrogen-bonded (HB)-silanols and physically adsorbed water, respectively, which is consistent with the values reported in most previous reports.[18,70,71] In addition, further distinction between HB-water (4.63 ppm) and free-water (5.08 ppm) could also be made because this peak vanished in the "SiNP-as received" after being mixed with DMSO and dried at 50 °C for 1 hour. The ^1H peak at 4.63 ppm still appeared in the $\{^1H–^{29}Si\}–^1H$ DCPi spectrum, suggesting this water is tightly bound to the SiNP surface. The $^1H–^1H$ RFDR spectrum (Fig. 2C) showed that the three aforementioned groups are in close proximity in space, probably bound by strong hydrogen bonds.

Determination of the proton spin–lattice relaxation constant (T_1^H, Fig. S2†) showed that the slowest relaxing group is the DMSO protons (T_1^H = 0.35 seconds). Based on the finding in Schmidt-Rohr's report,[28] τ_{rel} (Fig. 1B) in the multiCP block was therefore set to 0.7 seconds (2 × T_1^H) in order to allow ^1H to repolarize to 95% of the thermal equilibrium. For obtaining

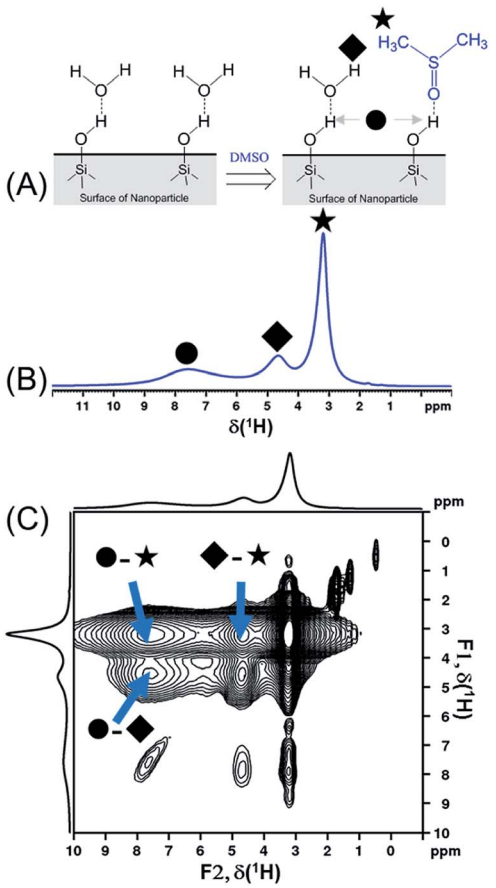

Fig. 2 (A) Schematic presentation of displacement of physically adsorbed water by dimethyl sulfoxide molecules on the silica nanoparticle surface. (B) ^{1}H one-pulse spectrum of DMSO-adsorbed SiNP (0.20 g SiNP + 0.11 g DMSO-h_6) obtained by ^{1}H one-pulse experiment (recycle delay = 4 seconds). The assignment of chemical shifts is as follow: ● δ(HB-silanol) = 7.50 ppm; ◆ δ(HB-water) = 4.63 ppm; ★ δ(HB-DMSO) = 3.16 ppm. (C) The ^{1}H–^{1}H radio-frequency-driven-recoupling (RFDR) correlation spectrum of DMSO-adsorbed SiNP (same sample as shown in (B)), using the pulse sequence of Fig. S1D† (mixing time = 18 ms). Note: three diagonal peaks in the region of 2 to 0 ppm might be assigned to isolated silanols and a very weak peak at 0.47 ppm that cannot be assigned.[15]

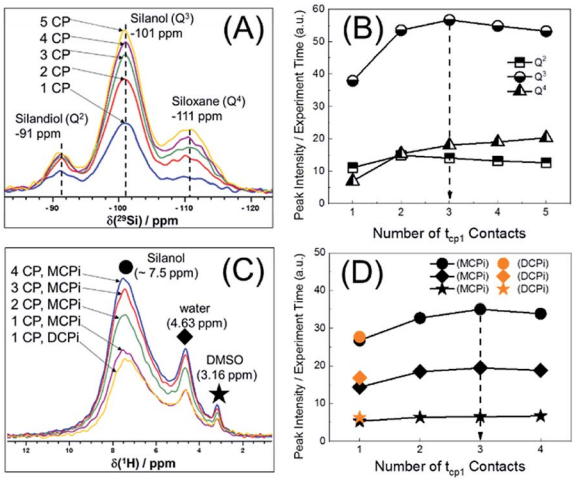

Fig. 3 Optimization of the number of CP contacts of MCPi experiment for the DMSO-h_6-adsorbed SiNP. (A) {^{1}H}–^{29}Si multiCP: RD = 4.0 s, contact time = 5 ms. (B) Evolution of ^{29}Si intensity with the number of contacts in ^{29}Si MultiCP experiment. (C) {^{1}H–^{29}Si}–^{1}H MCPi and DCPi spectra (RD = 4.0 s, $t_{cp1} = t_{cp2}$ = 5 ms). (D) Evolution of ^{1}H intensity with the number of contacts in MCPi and DCPi experiments.

optimal sensitivity, a relaxation delay of RD = 0.44 s (*i.e.* 1.26 × T_1^{H}) was initially chosen. However, in order to ensure that all protons have fully relaxed in cases where the T_1 (s) could not be clearly determined due to heavily overlapped ^{1}H peaks, we chose RD = 4.0 (the second to last points of the T_1 relaxation curves in Fig. S2†).

Another important parameter for running the {^{1}H–^{29}Si}–^{1}H experiment is the number of CP contacts (m of Fig. 1B). To figure out the optimal m value, ^{29}Si detected and ^{1}H detected experiments (Fig. S1B and C†) were performed on the same sample used in Fig. 2. The optimization process is shown in Fig. 3. There are pros and cons for higher values of m. Theoretically, more contacts (higher m values) result in more magnetization transfer from ^{1}H to ^{29}Si and therefore more backward magnetization transfer, as was experimentally confirmed (see Fig. 3A and C). However, for qualitative analysis (as in this case), higher values of m result in longer experiment time. In addition, the closer the ^{29}Si magnetization approaches the theoretical enhancement, the less efficient per time unit is each individual multiple CP step (Fig. 3B). Therefore, there is an optimal value for m, beyond which, there is no further marginal sensitivity gain per time unit (Fig. 3D). For the sample used in this case, the optimum was found to be m = 3, based on the maximum marginal gain of sensitivity of the silanol, water and DMSO signals (Fig. 3D).

With the key parameters being known (RD, τ_{rel} and m of Fig. 1), the sensitivities of the {^{1}H–^{29}Si}–^{1}H DCPi and MCPi techniques were compared. The two experiments were performed on the same sample (Fig. S4 and S5†) and the S/N ratios were calculated (Tables S1 and S2†). As expected, one immediately noticeable difference with the ^{1}H one-pulse is the relative intensities of the silanol, water and DMSO signals. In the one-pulse experiment (Fig. 2B), the relative peak intensities from highest to lowest is DMSO, water and silanol, whereas it is the opposite in the inverse detection experiments (Fig. 4A), which makes sense because the peak intensity of the one-pulse experiment are solely determined by concentration whereas it is modulated by inter-nuclear distance.

The overall sensitivity of each technique depends on the signal intensity, which was gained from one or multiple CP steps. Under three different conditions, the signals in the {^{1}H–^{29}Si}–^{1}H MCPi spectra were all stronger than in DCPi spectra. Overall, {^{1}H–^{29}Si}–^{1}H MCPi yields higher signal to noise ratio (S/N) than DCPi (Table S1 and Fig. S4†).

By normalizing the S/N ratios to experiment time per scan (*i.e.* the recycle delay + $t_{cp1} \times m + \tau_{sat} \times n + \tau_{rel} \times m + t_{cp2}$ + acquisition time), we could compare the intrinsic sensitivities of {^{1}H–^{29}Si}–^{1}H MCPi and DCPi (Table S1†) using eqn (1)–(6). In a fully relaxed spin system, the S/N is proportional to the square root of the number of scans (NS) (eqn (1)), which is proportional

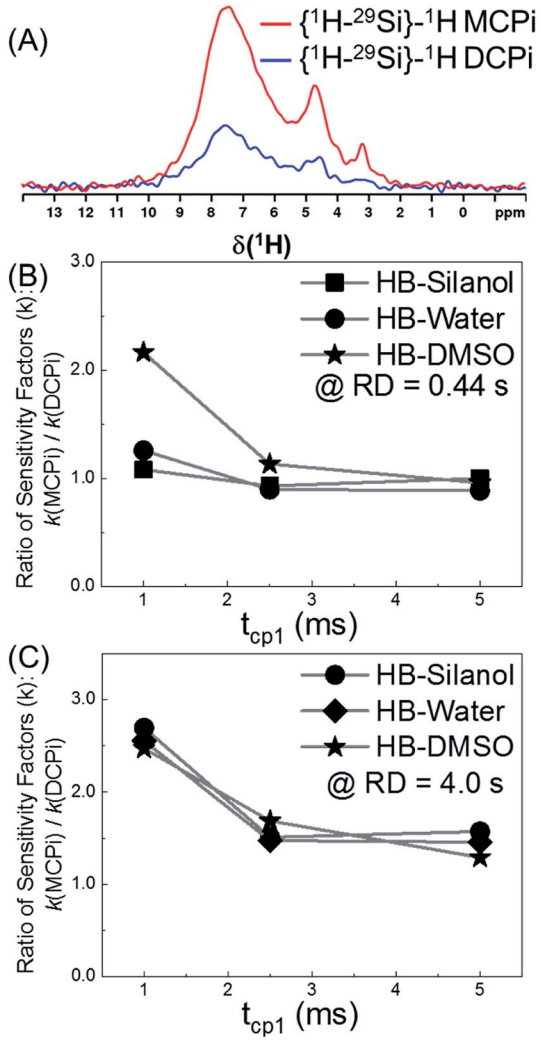

Fig. 4 The sensitivity comparison between $\{^1H–^{29}Si\}–^1H$ MCPi and DCPi. Same sample as used in Fig. 2B. (A) ^1H spectra obtained using the following parameters: RD = 0.44 s, t_{cp1} = 1 ms, t_{cp2} = 5 ms for both MCPi and DCPi, and m = 3 for MCPi. (B) Sensitivity ratio of MCPi over DCPi (k_{MCPi}/k_{DCPi}) when RD = 0.44 s (*i.e.* 1.26 × T_1^H), t_{cp1} = variable and t_{cp2} = 5 ms, and m = 3 for MCPi. (C) Same experiments as performed for (B), except RD = 4.0 s.

to the total experimental time (Expt, eqn (2)). Therefore, the S/N is proportional to the square root of the total experimental time (eqn (3)). Thus, the sensitivity of a given pulse sequence can be expressed as a sensitivity factor (k) times the square root of total experimental time (eqn (4)). Under the same experimental conditions (*i.e.* identical sample, temperature, receiver gain, number of scans, processing parameters, *etc.*), the k value can be determined by normalizing the S/N to total experimental time (eqn (5)). Hence, the time-efficiency of two sequences can be compared by comparing their k values (eqn (6)).

$$S/N \propto \sqrt{NS} \quad (1)$$

$$NS \propto Expt \quad (2)$$

$$S/N \propto \sqrt{Expt} \quad (3)$$

$$S/N = k \times \sqrt{Expt} \quad (4)$$

$$k = \frac{S/N}{\sqrt{Expt}} \quad (5)$$

$$\frac{k^{MCPi}}{k^{DCPi}} = \frac{S/N^{MCPi}}{S/N^{DCPi}} \times \frac{\sqrt{Expt}^{DCPi}}{\sqrt{Expt}^{MCPi}} \quad (6)$$

The t_{cp1} dependence of the k ratios between $\{^1H–^{29}Si\}–^1H$ MCPi and DCPi under variable t_{cp1} are shown in Fig. 4B and C. In NMR experiments, the sensitivity per time unit can be maximized by setting the recycle delay to 1.26 times the longest T_1 in a sample.[72–74] As shown in Fig. 4B, when a short relaxation delay of RD = 0.44 s was used, the overall sensitivity of MCPi for the molecule of interest, DMSO, was better or equivalent than that of DCPi over the t_{cp1} range. For silanol and water peaks, the sensitivity of MCPi is similar to that of DCPi, which makes sense because these groups are located closely to the surface silicon atoms so that magnetization transfer *via* CP is fast and a single CP contact is probably sufficient for transferring most of the proton magnetization to silicon. However, the optimum of 1.26 × T_1 is derived from an idealized situation where all the ^1H T_1 values in a sample can be clearly determined. Although this choice of recycle delay was applicable to the DMSO-adsorbed SiNP, that may be different in the case of composite materials where the ^1H peaks are heavily overlapped and some of the peaks might be so overwhelming that the T_1 of ^1H of other surface groups cannot be clearly determined. In that case, one needs to resort to using a long recycle delay in order to avoid saturating the surface groups (see the next section of a polymer–silica composite).

As shown in Fig. 4C, the results of RD = 4.0 s showed that the sensitivity improvement of $\{^1H–^{29}Si\}–^1H$ MCPi compared to DCPi, was nearly three-fold at t_{cp1} = 1 ms (meaning that it would take about 9 times longer time for DCPi to achieve the same S/N level as MCPi). At longer t_{cp1}, the improvement factor is around 1.5. Theoretically speaking, $\{^1H–^{29}Si\}–^1H$ MCPi would be even more efficient over the DCPi in situations where the proton spin–lattice relaxation in the rotating frame is much faster (shorter $T_{1\rho}$) (*i.e.* long spin locking pulse is inapplicable). In fact, a contact pulse of 1 ms is quite common.[28,38,50]

Moreover, we further explored the dependence of signal intensity on t_{cp2} in the experiments of $\{^1H–^{29}Si\}–^1H$ MCPi (Fig. S6†). The rates of S/N evolution with t_{cp2} differ between DMSO, silanol and water due to the difference in the distance relative to the silica surface. This behaviour is analogous to the one reported previously for the regular DCPi.[38]

3.2 Modified silica in a polymer matrix

In order to demonstrate the applicability of both MCPi and DCPi and their truly unique surface specificity in practical applications, we applied it to a polymer–silica composite (Fig. 5). In order to illustrate the surface specificity of our approach, silica was silanized by trimethylchlorosilane. The grafted trimethylsilyl groups increase the surface's

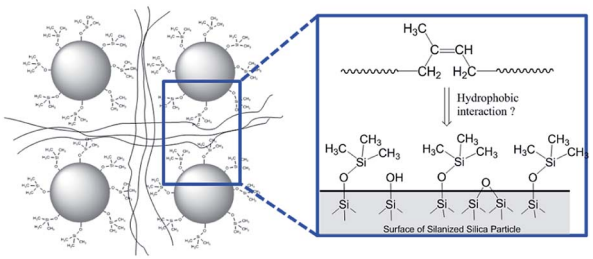

Fig. 5 Schematic representation of the silica surface in a polymer–silica composite, where the silica has been silanized by trimethylchlorosilane and the polymer is polyisoprene (see Experimental).

hydrophobicity compared to non-silanized silica, but no bonding between the silane and the polymer chains is created. The use of this mono-functional silane also prevents the occurrence of self-condensed polysiloxane chains, which might extend deeper into the polymer phase and entangle with the polymer chains, and achieve compatibility on those grounds.

The ^{29}Si spectra in Fig. 6A and B show that after the reaction with an excessive amount of silane, there is a significant amount of trimethylsilyl group grafted onto the silica surface and a noticeable decrease of the silanol peak (at −102 ppm).

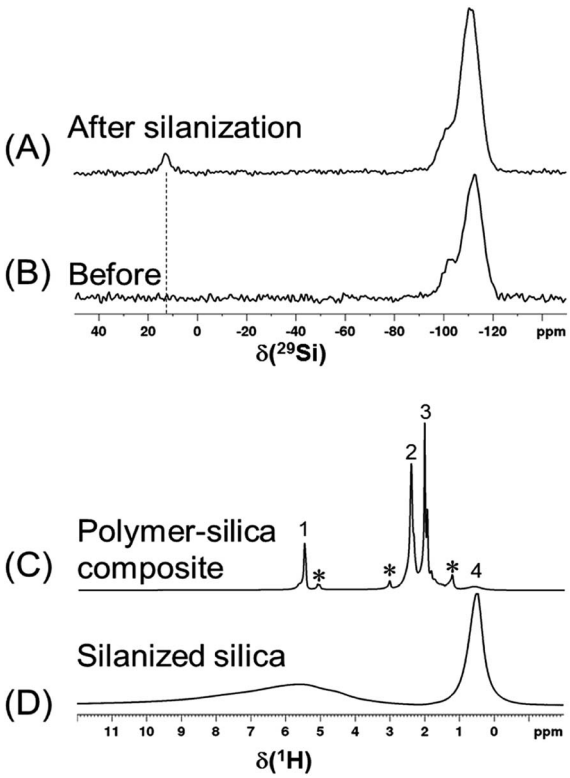

Fig. 6 (A, B) ^{29}Si DP spectra (RD = 120 s, MAS = 8 kHz) of silica before and after silanization. The number of scans is 512 and 600, respectively. The peak at 13 ppm is assigned to the trimethylsilyl group. (C, D) ^{1}H one-pulse spectra (RD = 4.0 s) of a silanized silica and the polymer–silanized silica composite. Peaks labelled 1, 2, 3, * and 4 are assigned to the vinyl, methylene, methyl groups of 1,4-polyisoprene, impurities of polyisoprene isomers and the trimethylsilyl group, respectively.

The ^{1}H spectra in Fig. 6C and D show that once the silanized silica was mixed with polymer, the ^{1}H peaks of polymer are so dominant that not all of the silanized silica ^{1}H peaks (3 to 10 ppm) can be distinguished. Thus, instead of performing a regular ^{1}H T_1 measurement, the recycle delay needed for reaching the thermal equilibrium was estimated to be >3.5 s in a set of ^{1}H one-pulse spectra with variable recycle delays (Fig. S7†). As a result, a recycle delay of 4.0 s and therefore an estimated inter-CP block delay τ_{rel} = 0.7 s were used for the following MCPi experiments. These two key parameters were confirmed to be efficient for building up the ^{29}Si magnetization rapidly (Fig. S8†).

The ^{1}H spectra in Fig. 7A were obtained by MCPi at various m values. As mentioned earlier, the MCPi pulse sequence of Fig. 1B actually can also achieve the function of DCPi simply by setting the multiCP loop number, $m = 1$ and inter-CP delay $\tau_{rel} = 0$, because the contribution of the first 90° pulse on ^{29}Si is negligible due to the long T_1 relaxation of ^{29}Si (Fig. 3C).

The sensitivity factor, k (see eqn (5)), for each m value was calculated plugging in the S/N ratios and the experiment duration (Expt) of Table S3.† As can be seen in Fig. 7B, the MCPi pulse sequence achieves a higher sensitivity by increasing the number of multiCP loops, m, with total mixing times that could not normally be achieved with a single contact. This result was overall in agreement with the results of the DMSO-adsorbed silica case. As mentioned in the Introduction, the observable inter-nuclear distance has an upper limit of a few nanometers. Even though a wide range of t_{cp2} values have been used (*i.e.* t_{cp2} = 5 ms in Fig. 7A and t_{cp2} = 1, 10 & 15 ms in Fig. S10†), none of

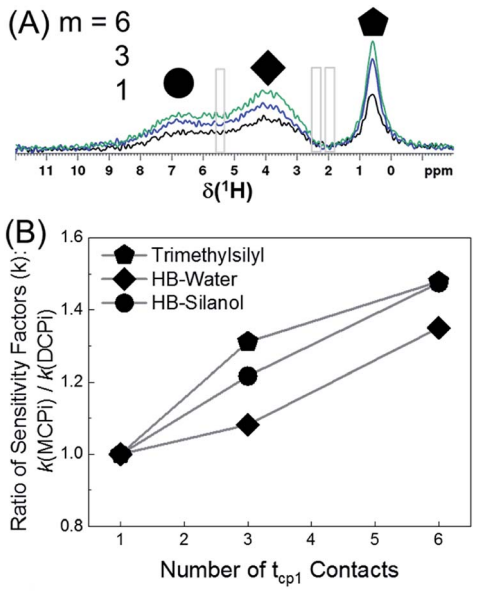

Fig. 7 (A) ^{1}H MCPi spectra of polymer–silica composite obtained by a slightly modified pulse sequence (Fig. S9†): RD = 4.0 s, $t_{cp1} = t_{cp2} = 5$ ms, τ_{rel} = 0.7 s and $m = 1$ (black), 3 (blue) and 6 (green). For $m = 1$, τ_{rel} = 0 s, this is effectively a DCPi experiment. Grey boxes are the regions where the polyisoprene signals would be expected. (B) The ratio of sensitivity factors k, between MCPi and DCPi calculated by eqn (6) using the S/N and experiment duration (Expt) values from Table S3.†

the polyisoprene ^{1}H peaks was observed, which is probably due to the weak dipolar coupling between the polyisoprene and silica surface.

4. Conclusions

In this work, we report a new solid-state NMR technique for characterizing the silica surface, $\{^{1}H–^{29}Si\}–^{1}H$ multiple cross polarization inverse detection (MCPi). This new technique combines the principle of multiple cross polarization and the recently reported $\{^{1}H–^{29}Si\}–^{1}H$ double cross polarization inverse detection (DCPi) technique. It was demonstrated in a model system composed of dimethyl sulfoxide adsorbed on silica nanoparticles that the sensitivity of MCPi was better or equivalent to DCPi under a wide range of experimental conditions. In a preliminary study of a polymer–silica composite sample, MCPi achieved a higher sensitivity than DCPi at long total mixing times, not attainable with a single contact.

Overall, MCPi is expected to perform better than DCPi in three situations: (1) the sample (*e.g.* composite materials) has multiple relatively fast ^{1}H spin–lattice relaxations in the rotating frame $T_{1\rho}^{H}$, (2) the silica surface is not (or only slightly) protonated, and (3) the overall silica content in the sample is very low. In the first situation, the built-up ^{29}Si magnetization will be constantly drained away due to $T_{1\rho}^{H}$. This will be attenuated using multiple, but short, cross polarisation steps, which will also be better suited for a variety of $T_{1\rho}^{H}$s. In the second scenario, *i.e.* when there are only few protons near the silica surface (*e.g.* in pyrogenic silica or modified silicas with few grafted or adsorbed groups), the proton–silicon dipolar coupling is weaker and the CP kinetics is slower. Therefore, the total contact time has to be very long, which can be safely achieved by a multiCP block. In the third case, when the total amount of silica in sample, *e.g.* a composite material, is low, therefore requiring long experimental time in order to achieve signal-to-noise ratios suitable for analysis, even a small sensitivity enhancement means significant saving of experiment time.

Conflicts of interest

There are no conflicts to declare.

Acknowledgements

The work is funded by the Luxembourg National Research Fund (FNR) under the project number IPBG16/11514551/TireMat-Tech. Support for implementing the $\{^{1}H\}–^{29}Si$ multiCP sequence by Dr Gerhard Althoff-Ospelt is also gratefully acknowledged. The authors would like to thank Mr Enzo Moretto for helpful discussion on the synthesis of silane-modified silicas.

Notes and references

1 J. K. Norskov and C. H. Christensen, *Science*, 2006, **312**, 1322.
2 J. Gong, H. Yue, Y. Zhao, S. Zhao, L. Zhao, J. Lv, S. Wang and X. Ma, *J. Am. Chem. Soc.*, 2012, **134**, 13922–13925.
3 S. Kattel, P. J. Ramírez, J. G. Chen, J. A. Rodriguez and P. Liu, *Science*, 2017, **355**, 1296.
4 A. Wong, Q. Liu, S. Griffin, A. Nicholls and J. R. Regalbuto, *Science*, 2017, **358**, 1427.
5 D. Strmcnik, K. Kodama, D. van der Vliet, J. Greeley, V. R. Stamenkovic and N. M. Marković, *Nat. Chem.*, 2009, **1**, 466–472.
6 W. Li, A. Dolocan, P. Oh, H. Celio, S. Park, J. Cho and A. Manthiram, *Nat. Commun.*, 2017, **8**, 14589.
7 H. Gao, L. Xue, S. Xin and J. B. Goodenough, *Angew. Chem., Int. Ed.*, 2018, **57**, 5449–5453.
8 J. Nawrocki, M. Rigney, A. McCormick and P. W. Carr, *J. Chromatogr. A*, 1993, **657**, 229–282.
9 J. Nawrocki, *J. Chromatogr. A*, 1997, **779**, 29–71.
10 Y. Song, Y. Shen, H. Liu, Y. Lin, M. Li and C.-W. Nan, *J. Mater. Chem.*, 2012, **22**, 16491–16498.
11 B. P. Kapgate, C. Das, D. Basu, A. Das and G. Heinrich, *J. Elastomers Plast.*, 2013, **47**, 248–261.
12 R. Semino, N. A. Ramsahye, A. Ghoufi and G. Maurin, *ACS Appl. Mater. Interfaces*, 2016, **8**, 809–819.
13 A. K. Clarke, M. J. James, P. O'Brien, R. J. K. Taylor and W. P. Unsworth, *Angew. Chem., Int. Ed.*, 2016, **55**, 13798–13802.
14 C. M. Crudden, M. Sateesh and R. Lewis, *J. Am. Chem. Soc.*, 2005, **127**, 10045–10050.
15 J. Brus and J. Dybal, *Polymer*, 2000, **41**, 5269–5282.
16 Z. Teng, C. Wang, Y. Tang, W. Li, L. Bao, X. Zhang, X. Su, F. Zhang, J. Zhang, S. Wang, D. Zhao and G. Lu, *J. Am. Chem. Soc.*, 2018, **140**, 1385–1393.
17 J. Brus, W. Albrecht, F. Lehmann, J. Geier, J. Czernek, M. Urbanova, L. Kobera and A. Jegorov, *Mol. Pharm.*, 2017, **14**, 2070–2078.
18 C. E. Bronnimann, R. C. Zeigler and G. E. Maciel, *J. Am. Chem. Soc.*, 1988, **110**, 2023–2026.
19 J. Brus and J. Dybal, *Macromolecules*, 2002, **35**, 10038–10047.
20 G. E. Maciel, Silica Surfaces: Characterization, in *eMagRes* ed. R. K. Harris and R. L. Wasylishen, 2007, DOI: 10.1002/9780470034590.emrstm0504.
21 G. E. Maciel and D. W. Sindorf, *J. Am. Chem. Soc.*, 1980, **102**, 7606–7607.
22 G. E. Michael, D. W. Sindorf and V. J. Bartuska, *J. Chromatogr. A*, 1981, **205**, 438–443.
23 D. W. Sindorf and G. E. Maciel, *J. Am. Chem. Soc.*, 1981, **103**, 4263–4265.
24 B. Pfleiderer, K. Albert, E. Bayer, L. van de Ven, J. de Haan and C. Cramers, *J. Phys. Chem.*, 1990, **94**, 4189–4194.
25 D. R. Spearing, I. Farnan and J. F. Stebbins, *Phys. Chem. Minerals*, 1992, **19**, 307–321.
26 S. Inagaki, I. Kawamura, Y. Sasaki, K. Yoshida, Y. Kubota and A. Naito, *Phys. Chem. Chem. Phys.*, 2013, **15**, 13523–13531.
27 S. Zhang, X. Wu and M. Mehring, *Chem. Phys. Lett.*, 1990, **166**, 92–94.
28 R. L. Johnson and K. Schmidt-Rohr, *J. Magn. Reson.*, 2014, **239**, 44–49.
29 H. Liu, X. Zhou, Q. Chen and S. Zhang, *Chem. Phys. Lett.*, 2017, **679**, 233–236.

30 P. Duan and K. Schmidt-Rohr, *J. Magn. Reson.*, 2017, **285**, 68–78.
31 J. Raya and J. Hirschinger, *J. Magn. Reson.*, 2017, **281**, 253–271.
32 S. Smet, P. Verlooy, F. Saïdi, F. Taulelle, J. A. Martens and C. Martineau-Corcos, *Magn. Reson. Chem.*, 2019, **57**, 224–229.
33 M. Lelli, D. Gajan, A. Lesage, M. A. Caporini, V. Vitzthum, P. Miéville, F. Héroguel, F. Rascón, A. Roussey, C. Thieuleux, M. Boualleg, L. Veyre, G. Bodenhausen, C. Coperet and L. Emsley, *J. Am. Chem. Soc.*, 2011, **133**, 2104–2107.
34 A. J. Rossini, A. Zagdoun, M. Lelli, D. Gajan, F. Rascón, M. Rosay, W. E. Maas, C. Copéret, A. Lesage and L. Emsley, *Chem. Sci.*, 2012, **3**, 108–115.
35 T. H. Walter, G. L. Turner and E. Oldfield, *J. Magn. Reson.*, 1969, **76**, 106–120.
36 F. A. Perras, Z. Wang, P. Naik, I. I. Slowing and M. Pruski, *Angew. Chem., Int. Ed.*, 2017, **56**, 9165–9169.
37 H. D. Morris and P. D. Ellis, *J. Am. Chem. Soc.*, 1989, **111**, 6045–6049.
38 N. Baccile, G. Laurent, C. Bonhomme, P. Innocenzi and F. Babonneau, *Chem. Mater.*, 2007, **19**, 1343–1354.
39 M. P. Hanrahan, E. L. Fought, T. L. Windus, L. M. Wheeler, N. C. Anderson, N. R. Neale and A. J. Rossini, *Chem. Mater.*, 2017, **29**, 10339–10351.
40 J. Trebosc, J. W. Wiench, S. Huh, V. S. Lin and M. Pruski, *J. Am. Chem. Soc.*, 2005, **127**, 3057–3068.
41 J. W. Wiench, V. S. Lin and M. Pruski, *J. Magn. Reson.*, 2008, **193**, 233–242.
42 W. J. Malfait, S. Zhao, R. Verel, S. Iswar, D. Rentsch, R. Fener, Y. Zhang, B. Milow and M. M. Koebel, *Chem. Mater.*, 2015, **27**, 6737–6745.
43 P. Brunner, M. Reinhold and R. R. Ernst, *J. Chem. Phys.*, 1980, **73**, 1086–1094.
44 Y. Ishii and R. Tycko, *J. Magn. Reson.*, 2000, **142**, 199–204.
45 Y. Ishii, J. P. Yesinowski and R. Tycko, *J. Am. Chem. Soc.*, 2001, **123**, 2921–2922.
46 A. K. Khitrin and B. M. Fung, *J. Magn. Reson.*, 2001, **152**, 185–188.
47 J. W. Wiench, C. E. Bronnimann, V. S. Y. Lin and M. Pruski, *J. Am. Chem. Soc.*, 2007, **129**, 12076–12077.
48 D. Carnevale, X. Ji and G. Bodenhausen, *J. Chem. Phys.*, 2017, **147**, 184201.
49 J. S. Bridel, T. Azaïs, M. Morcrette, J. M. Tarascon and D. Larcher, *Chem. Mater.*, 2010, **22**, 1229–1241.
50 N. Folliet, C. Roiland, S. Bégu, A. Aubert, T. Mineva, A. Goursot, K. Selvaraj, L. Duma, F. Tielens, F. Mauri, G. Laurent, C. Bonhomme, C. Gervais, F. Babonneau and T. Azaïs, *J. Am. Chem. Soc.*, 2011, **133**, 16815–16827.
51 S. Cadars, R. Guégan, M. N. Garaga, X. Bourrat, L. Le Forestier, F. Fayon, T. V. Huynh, T. Allier, Z. Nour and D. Massiot, *Chem. Mater.*, 2012, **24**, 4376–4389.
52 B. Thomas, T. Coradin, G. Laurent, R. Valentin, Z. Mouloungui, F. Babonneau and N. Baccile, *RSC Adv.*, 2012, **2**, 426–435.
53 K. Mao, T. Kobayashi, J. W. Wiench, H. T. Chen, C. H. Tsai, V. S. Lin and M. Pruski, *J. Am. Chem. Soc.*, 2010, **132**, 12452–12457.
54 K. Hara, S. Akahane, J. W. Wiench, B. R. Burgin, N. Ishito, V. S. Y. Lin, A. Fukuoka and M. Pruski, *J. Phys. Chem. C*, 2012, **116**, 7083–7090.
55 A. R. Mouat, T. Kobayashi, M. Pruski, T. J. Marks and P. C. Stair, *J. Phys. Chem. C*, 2017, **121**, 6060–6064.
56 T. Kobayashi and M. Pruski, *ACS Catal.*, 2019, **9**, 7238–7249.
57 A. G. M. Rankin, P. B. Webb, D. M. Dawson, J. Viger-Gravel, B. J. Walder, L. Emsley and S. E. Ashbrook, *J. Phys. Chem. C*, 2017, **121**, 22977–22984.
58 S. K. Parida, S. Dash, S. Patel and B. K. Mishra, *Adv. Colloid Interface Sci.*, 2006, **121**, 77–110.
59 J. K. Moon, D. K. Keum and W. K. Lee, *Korean J. Chem. Eng.*, 1989, **6**, 172–178.
60 Z. Yang, Q. Li, R. Hua, M. R. Gray and K. C. Chou, *J. Phys. Chem. C*, 2009, **113**, 20355–20359.
61 Y. Wu, M. Zhang, H. Zhao, S. Yang and A. Arkin, *RSC Adv.*, 2014, **4**, 61256–61267.
62 J. Shi, L. Gong, S. Sun, Z. Huang, B. Ding and J. Yao, *RSC Adv.*, 2019, **9**, 25326–25335.
63 A. M. Bodratti, B. Sarkar, D. Song, M. Tsianou and P. Alexandridis, *J. Dispersion Sci. Technol.*, 2015, **36**, 1–9.
64 H. Bessaies-Bey, J. Fusier, M. Hanafi, S. Zhang, M. Destarac, S. Jouenne, N. Passade-Boupat, F. Lequeux, J. B. d'Espinose de Lacaillerie and N. Sanson, *Colloids Surf., A*, 2019, **579**, 123673.
65 J. Ghodbane and R. Denoyel, *Colloids Surf., A*, 1997, **127**, 97–104.
66 B. R. Postmus, F. A. M. Leermakers, L. K. Koopal and M. A. Cohen Stuart, *Langmuir*, 2007, **23**, 5532–5540.
67 R. Simonutti, A. Comotti, F. Negroni and P. Sozzani, *Chem. Mater.*, 1999, **11**, 822–828.
68 H. Dohi and S. Horiuchi, *Langmuir*, 2007, **23**, 12344–12349.
69 I. Klur, J. F. Jacquinot, F. Brunet, T. Charpentier, J. Virlet, C. Schneider and P. Tekely, *J. Phys. Chem. B*, 2000, **104**, 10162–10167.
70 A. J. Vega and G. W. Scherer, *J. Non-Cryst. Solids*, 1989, **111**, 153–166.
71 J.-B. d'Espinose de la Caillerie, M. R. Aimeur, Y. E. Kortobi and A. P. Legrand, *J. Colloid Interface Sci.*, 1997, **194**, 434–439.
72 Y. Q. Ye, M. Malon, C. Martineau, F. Taulelle and Y. Nishiyama, *J. Magn. Reson.*, 2014, **239**, 75–80.
73 Y. Q. Ye, C. Martineau-Corcos, F. Taulelle and Y. Nishiyama, *J. Magn. Reson.*, 2018, **294**, 122–127.
74 Y. Nishiyama, *Experimental Approaches of NMR Spectroscopy: Methodology and Application to Life Science and Materials Science*, Springer Nature, Singapore, 2018, pp. 180–181.